

# Fractional anisotropy as a tracer of cosmic voids

Sebastian Bustamante <sup>\*1</sup>, Jaime E. Forero-Romero <sup>2</sup>

<sup>1</sup>*Instituto de Física - FCEN, Universidad de Antioquia, Calle 67 No. 53-108, Medellín, Colombia*

<sup>2</sup>*Departamento de Física, Universidad de los Andes, Cra. 1 No. 18A-10, Edificio Ip, Bogotá, Colombia*

21 October 2014

## ABSTRACT

Finding and characterizing voids in the large scale structure of the universe is an important task in cosmological studies. In this paper we present a novel approach to find voids in cosmological simulations. It is based on algorithms that use the tidal and the velocity shear tensors to define the cosmic web. Voids are identified using the fractional anisotropy (FA) computed from the eigenvalues of each web scheme. We define the void boundaries using a watershed transform based on the local minima of the FA; the boundaries are regions where the FA is maximized, corresponding to walls and filaments. This void definition does not have any free parameter and does not make any assumption on the shape or structure of the voids. We test the method on the Bolshoi simulation and report on the density and velocity profiles for the voids found using this new scheme.

**Key words:** Cosmology: theory - large-scale structure of Universe - Methods: data analysis - numerical - N-body simulations

## 1 INTRODUCTION

Since voids were discovered in the first compiled galaxy surveys (Chincarini & Rood 1975; Gregory & Thompson 1978; Einasto et al. 1980a,b; Kirshner et al. 1981, 1987), they have been identified, along with the filamentary and hierarchically clustered nature of the Cosmic Web, as one of the most striking features of the Megaparsec Universe (Bond et al. 1996). Nevertheless, due to the large volume extension of void regions ( $\sim 5 - 10 \text{ Mpc} h^{-1}$ ), statistically meaningful catalogues of voids (Pan et al. 2012; Sutter et al. 2012; Nadathur & Hotchkiss 2014) only have become available after modern large galaxy surveys like the two-degree field Galaxy Redshift Survey (Colless et al. 2001, 2003) and the Sloan Digital Sky Survey (York et al. 2000; Abazajian et al. 2003), thereby triggering a plethora of more refined observational and statistical studies of voids throughout the last decade (Hoyle & Vogeley 2004; Croton et al. 2004; Rojas et al. 2005; Ceccarelli et al. 2006; Patiri et al. 2006; Tikhonov 2006; Patiri et al. 2006; Tikhonov 2007; von Benda-Beckmann & Müller 2008; Foster & Nelson 2009; Ceccarelli et al. 2013; Sutter et al. 2014).

On the theoretical side, early descriptions of the evolution of the large-scale Universe, based on gravitational instabilities in primordial stages and led by the seminal work of Zel'dovich (1970), are consistent with the Cosmic Web picture, where planar pancake-like regions of mat-

ter enclose enormous underdense voids and are bordered, in turn, by thin filaments and high-density clumpy knots (Bond et al. 1996). First theoretical models for describing formation, dynamics and properties of voids (Hoffman & Shaham 1982; Icke 1984; Bertschinger 1985; Blumenthal et al. 1992) were dramatically complemented and extended by first numerical studies based on simulations (Martel & Wasserman 1990; Regos & Geller 1991; van de Weygaert & van Kampen 1993; Dubinski et al. 1993). This tendency of using numerical data from N-body simulations, fuelled by last generation computing systems and ever more efficient numerical algorithms, has become increasingly common in the last years as a powerful analysis toolkit of cosmic voids (for an extensive compilation of previous numerical works, see Colberg et al. (2008)).

At present, studying voids may be considered as a three-fold enterprise (Platen et al. 2007): first, they are a key ingredient of the Cosmic Web as they dominate almost the entire volume distribution at large-scales and additionally, they compensate overdense structures in the total budget of matter. This implies that a full understanding of their evolution and properties is essential for fathoming the high complexity of the Cosmic Web. Second, they provide a valuable resource for inferring and probing cosmological parameters as their structure and dynamics are highly determined by these values. Third, they constitute an unique and still largely pristine environment in which can be tested galaxy evolution.

Although a visual recognition of voids in galaxy surveys

\* sebastian.bustamante@udea.edu.co

and simulations is possible in most cases, a formal systematic identification is necessary for statistically meaningful studies. However, a basic yet essential issue remains regarding the definition itself of what a void is. There is not a general consensus about an unambiguous definition of cosmic voids and therefore, there can be found many different void finding techniques throughout the literature (for a detailed comparison of different schemes, see the Void Finder Comparison Project Colberg et al. (2008)). In spite of the diversity of existing schemes, they can be roughly classified into two main types: first, geometric schemes based on point spatial or redshift distribution of galaxies in surveys or catalogues of dark matter halos in simulations (Kauffmann & Fairall 1991; Müller et al. 2000; Gottlöber et al. 2003; Hoyle & Vogeley 2004; Brunino et al. 2007; Foster & Nelson 2009; Micheletti & et al. 2014; Sutter et al. 2014), and second, schemes based on the smooth and continuous matter density field either from simulations or from reconstruction procedures on surveys (Plionis & Basilakos 2002; Colberg et al. 2005; Shandarin et al. 2006; Platen et al. 2007; Neyrinck 2008; Neyrinck et al. 2013; Ricciardelli et al. 2013).

Here we introduce a new tracer of the structure of cosmic voids built from two tensorial web schemes, i.e. the Tweb, based on the Hessian of the gravitational potential or tidal tensor (Hahn et al. 2007; Forero-Romero et al. 2009), and the Vweb, based on the velocity shear tensor (Hoffman et al. 2012). These web schemes classify the Cosmic Web into four different types of environment depending on the counting of the number of eigenvalues below an user-defined threshold ( $\lambda_{th}$ ), namely voids (3 eigenvalues below  $\lambda_{th}$ ), sheets (2), filaments (1) and knots or clusters (0). The tidal and the shear tensors have proven to be more fundamental than the density field as they also trace the collapsing or expanding nature of the matter field, which ultimately is what defines the underlying dynamics of the Cosmic Web. Furthermore, the density field is degenerated regarding the defined types of environment (Hahn et al. 2007), which implies that is not possible to assign a priori a range of density values to each of them. This yields that the usually adopted definition of voids as simply underdense regions in the large-scale matter distribution, is not precise enough as it excludes a proper description of the internal structure of voids.

Following the recent trend of using digital image-processing techniques developed in other disciplines (e.g. medical sciences and computer imaging) for analysing the structure of the Cosmic Web, we propose here, much in the same way as Libeskind et al. (2013), the fractional anisotropy (FA) as a tracer of the internal structure and the outline of cosmic voids. The FA was initially introduced by Bassler (1995) for quantifying the anisotropy degree of the diffusivity of water molecules through cerebral tissue in nuclear magnetic resonance imaging. In this context we use the same quantity for determining the anisotropy degree of the local environment from either the orbital dynamics as set by the eigenvalues of the tidal tensor (Tweb), or the dynamics of the velocity field as set by the eigenvalues of the shear tensor (Vweb). In both cases, the FA is not determined directly from the density field, it hence is suitable for describing both, the structure of high non-linear regions (e.g. filaments, knots and very dense walls) as well as the fainter substructure exhibited by quasi-linear regions like voids.

Once established the FA as the tracer field of cosmic

voids, we proceed to identify individual voids as basins of local minima. For this purpose we implement a technique developed by Beucher & Lantuejoul (1979) and Beucher & Meyer (1993) and widely used in the field of image analysis and mathematical morphology, i.e. the *watershed transform algorithm*. This technique has been already implemented on void finding schemes by Platen et al. (2007) and Neyrinck (2008) with very interesting results, where individual voids are identified as catching basins of local minima of the density field. The appeal of this algorithm consists in that is parameter-free and does not require any assumption on the shape and morphology of voids. Although we use a *cloud-in-cell* (CIC) algorithm on a Cartesian mesh for estimating the density and tensor fields, instead of the more sophisticated *Delaunay tessellation for field estimator* (DTFE) technique (Schaap & van de Weygaert 2000), our implementation of the watershed transform should not be significantly affected as we are interested in quasi-linear regions where the CIC gives similar estimations.

This paper is organized as follows. In section 2 we describe the used simulation for testing our void finding algorithm, i.e. the Bolshoi simulation. A detailed description of these methods is presented in section 3. In section 4 we describe how the FA can be used for tracing the structure of voids. Once obtained meaningful catalogues of voids for each scheme, we proceed to compare some typical and general interest properties of voids such as volume functions, distributions of size and density and velocity profiles. This is done in section 5. Finally in section 6 we analyse and evaluate our findings.

## 2 THE SIMULATION

We use here an unconstrained cosmological simulation (the Bolshoi simulation) to identify the possible large scale environment and the distribution of cosmic voids at  $z = 0$ . The Bolshoi simulation follows the non-linear evolution of a dark matter density field on a cubic volume of size  $250h^{-1}\text{Mpc}$  sampled with  $2048^3$  particles. The cosmological parameters in the simulation are  $\Omega_m = 0.27$ ,  $\Omega_\Lambda = 0.73$ ,  $h = 0.70$ ,  $n = 0.95$  and  $\sigma_8 = 0.82$  for the matter density, cosmological constant, dimensionless Hubble parameter, spectral index of primordial density perturbations and normalization for the power spectrum respectively, consistent with the seventh year of data of the Wilkinson Microwave Anisotropy Probe (WMAP) (Jarosik et al. 2011). For more detailed technical information about the simulation, see Klypin et al. (2011).

For estimating the density and velocity fields we use a *cloud-in-cell* (CIC) algorithm onto a grid of  $256^3$  cells, corresponding to a resolution of  $0.98h^{-1}\text{Mpc}$  per cell side. Then, through finite-differences and FFT methods the tidal and shear tensors are computed. Finally, the eigenvalues and eigenvectors of the tensor are obtained for each cell of the grid. Neglecting substructures presented below Megaparsec scales and taking into account our focus in voids, which are a prominent characteristic of the Megaparsec Universe, we apply a Gaussian softening of one cell to all fields.

### 3 ALGORITHMS TO QUANTIFY THE COSMIC WEB

#### 3.1 The tidal web (Tweb)

This scheme was initially proposed by Hahn et al. (2007) as a novel alternative for classifying the Cosmic Web based on the tidal tensor, that is somehow more fundamental than the density field as it also allows to quantify the orbital dynamics of the matter field. This approach consists of a second-order expansion of the equations of motion around local minima of the gravitational potential and then extended to any position. The second-order term corresponds to the tidal tensor, which is defined as the Hessian matrix of the normalized gravitational potential

$$T_{\alpha\beta} = \frac{\partial^2 \phi}{\partial x_\alpha \partial x_\beta} \quad (1)$$

where the physical gravitational potential has been rescaled by a factor  $4\pi G\bar{\rho}$  in such a way that  $\phi$  satisfies the following equation

$$\nabla^2 \phi = \delta, \quad (2)$$

with  $\bar{\rho}$  the average density in the Universe,  $G$  the gravitational constant and  $\delta$  the dimensionless matter overdensity.

Since the tidal tensor can be represented in any cell by a real and symmetric  $3 \times 3$  matrix, it is ensured the possibility to diagonalize it and obtain three real eigenvalues  $\lambda_1 \geq \lambda_2 \geq \lambda_3$ . This set of eigenvalues can be used as indicators of the local orbital stability in each proper direction, which in turn can be translated into a classification scheme of the Cosmic Web. A counting of the number of positive (stable) or negative (unstable) eigenvalues allows to catalogue a single cell into one of the next four types of environment: voids (3 negatives eigenvalues), sheets (2), filaments (1) and knots (0). A significant improvement to this scheme was introduced by Forero-Romero et al. (2009) by means of a relaxation of the stability criterion. The relative strength of each eigenvalue is no longer defined by the sign, but instead by a threshold value  $\lambda_{th}$  that can be tuned in such a way that the visual impression of the web-like matter distribution is reproduced.

#### 3.2 The velocity web (Vweb)

We also use a kinematical scheme to define the Cosmic Web environment in the simulation. The scheme has been thoroughly described in Hoffman et al. (2012) and applied to study the shape and spin alignment in the Bolshoi simulation in Libeskind et al. (2013). We refer the reader to these papers to find a detailed description of the algorithm, its limitations and capabilities. The Vweb scheme for environment finding is based on the local velocity shear tensor calculated from the smoothed dark matter velocity field in the simulation. The central quantity is given by the following dimensionless expression

$$\Sigma_{\alpha\beta} = -\frac{1}{2H_0} \left( \frac{\partial v_\alpha}{\partial x_\beta} + \frac{\partial v_\beta}{\partial x_\alpha} \right) \quad (3)$$

where  $v_\alpha$  and  $x_\alpha$  represent the  $\alpha$  component of the comoving velocity and position, respectively. Like the tidal tensor,  $\Sigma_{\alpha\beta}$  can be represented by a  $3 \times 3$  symmetric matrix with real values, hence diagonalizing it is obtained three real eigenvalues  $\lambda_1 \geq \lambda_2 \geq \lambda_3$  whose sum (the trace of  $\Sigma_{\alpha\beta}$ ) is proportional to the divergence of the local velocity field smoothed on the physical scale  $\mathcal{R}$ .

In the same way, the relative strength of the three eigenvalues with respect to a threshold value  $\lambda_{th}$  allows for the local classification of the matter distribution into the previous four web types. For the threshold choosing in both schemes, the Tweb and the Vweb, it is usual to fine-tuning the value in such a way that the visual appearance of the Cosmic Web as seen in simulations and galaxy surveys is reproduced. However, we do not take this approach here, instead we propose a novel approach for the threshold choosing based on the maximization of the fractional anisotropy field occurring in filaments and very dense walls.

## 4 FINDING VOIDS

#### 4.1 Fractional anisotropy as tracer of voids

The fractional anisotropy (FA), as developed by Bassler (1995), was conceived to quantify the anisotropy degree of a diffusion process, e.g. the diffusivity of water molecules through cerebral issue in nuclear magnetic resonance imaging. Here we propose the FA, much in the same way as Libeskind et al. (2013), as a tracer of cosmic voids.

$$FA = \frac{1}{\sqrt{3}} \sqrt{\frac{(\lambda_1 - \lambda_3)^2 + (\lambda_2 - \lambda_3)^2 + (\lambda_1 - \lambda_2)^2}{\lambda_1^2 + \lambda_2^2 + \lambda_3^2}} \quad (4)$$

where the eigenvalues are taken from either the Tweb or the Vweb (FA-Tweb and FA-Vweb respectively). Such as it is defined,  $FA = 0$  corresponds with an isotropic dynamic and  $FA = 1$  with a highly anisotropic distribution.

In left panels of Fig. 3 we calculate the FA for both web schemes and the logarithmic density field for a slide of the simulation. Some important points can be concluded of this figure.

- Voids display a highly isotropic expanding dynamic at their centres, becoming gradually more anisotropic at outer regions.
- Knots feature with very isotropic collapses. For the Tweb, the FA exhibits very narrow distribution around knots whereas for the Vweb, these distributions are more spread out, thereby indicating strong differences between the density and the velocity fields in highly non-linear regions.
- The filamentary structure of the Cosmic Web is very well traced by high FA values (black regions), thus indicating very anisotropic dynamics for sheets and filaments.
- The density field poorly traces the Cosmic Web. This is a somehow expected result due to the semi-infinite range of the density field, what makes more difficult to trace structures.

Some of these results are consistent with those of Libeskind et al. (2013). Finally, from Fig. 3 we conclude that the FA, unlike the density field, displays a non-monotonic

behaviour, where low values are characteristic of central regions of voids, reaching high values in sheets and filaments and becoming low again in knots.

For both web schemes, voids are regions where  $\lambda_3 \leq \lambda_2 \leq \lambda_1 \leq \lambda_{th}$ . This implies that the outlines of voids are completely fixed by the relative strength of the  $\lambda_1$  eigenvalue with respect to the threshold value. Therefore, as we increase/decrease the threshold value  $\lambda_{th}$ , voids expand/diminish progressively through contours of  $\lambda_1$ . In Fig. 1 we calculate the distribution of the FA as well as of the density field with respect to  $\lambda_1$  for both web schemes over all cells of the simulation.

From Fig. 1 we conclude that the FA is a good tracer of voids as is perfectly correlated with low values of  $\lambda_1$ . Then, it reaches a maximum value, namely sheets and filaments, for finally reaching knots, which feature low FA values. This behaviour can be thought as a sort of one-dimensional tomography of the Cosmic Web. This characteristic allows us to propose an optimal threshold value for both web schemes where the FA is maximized. Specifically we propose a value of  $FA = 0.95$ , corresponding with a threshold  $\lambda_{opt}^T = 0.265$  for the Tweb and  $\lambda_{opt}^V = 0.175$  for the Vweb. For a threshold above these values, voids would span over very anisotropic regions, which should correspond to sheets and filaments. A threshold below would imply very low volume filling fractions of voids and dominant sheets. Finally from the same figure, the density field do not correlate well with  $\lambda_1$  (as calculated for both web schemes). Moreover, due to its monotonic increase, an estimate of a optimal threshold is not as clear as for the FA.

Once set the optimal thresholds for the web schemes, we proceed in Fig. 2 to sample the FA along with the prolateness for a random sample of cells classified into the four environments. Then, we associate a spheroidal geometry with different ranges of these properties in order to illustrate the underlying local dynamics of the sampled cells.

From this figure we conclude that sheets displays, as expected, very anisotropic distributions, namely above  $FA = 0.95$ . They are also biased towards oblate geometries, however there are some elongated sheets as well. Filaments are not as anisotropic as sheets, ranging from middle up to high FA values. They exhibit prolate geometries, but a considerable amount of them are biased towards slightly more oblate values. Voids and knots are the only environments featuring with low FA values, thus indicating very isotropic expanding/collapsing dynamics at their centres. However, voids span over a very wide range of FA and geometries, whereas knots only span over low to middle FA values and display a biased oblate geometry.

## 4.2 Identifying void regions through web schemes

## 5 PROPERTIES OF VOIDS

Once defined our method to classify bulk voids based upon web classification schemes of the cosmic web, we proceed to analyse some physical properties in order to compare their consistency with the geometry of voids as quantified by our method and by density-based schemes. Next, through the reduced inertia tensor we quantify the shape distribution of voids. Finally, we compute numerical radial profiles of density and peculiar velocity of bulk voids.

## 5.1 Statistics of halos in voids

One of the main challenges in observational void finding is the discrete nature of galaxy surveys

we calculate contours of discrete fields like the median mass and the local number of local dark matter halos and , like the inertia values, the density and peculiar velocities profiles as calculated over the grid and profiles of number of halos.

## 5.2 Density profile of voids

Describing the density profiles of voids is quite important in order to compare and match simulation with observational surveys, allowing possible constrains for different cosmology models [Hamaous, et.al 2014]. Here, and taking into account the previous results, we rather use an ellipsoidal approximation to describe and fit the shape of bulk voids, so we use the next ellipsoidal radial coordinate to describe density profiles.

$$r^2 = \frac{x^2}{\tau_1^2} + \frac{y^2}{\tau_2^2} + \frac{z^2}{\tau_3^2}, \quad 0 \leq r \leq 1 \quad (5)$$

where we take the principal moments of inertia  $\{\tau_i\}$  as the lengths of the principal axes of the ellipsoid and each one of the cartesian coordinates as measured in the rotated frame of each void.

We use the same analytic density profile that [Hamaous, et.al 2014] to fit the numerical density profiles of our voids.

$$\delta_v(r) = \delta_c \frac{1 - (r/r_s)^\alpha}{1 + (r/r_v)^\beta} \quad (6)$$

## 6 CONCLUSIONS

## ACKNOWLEDGMENTS

## REFERENCES

- Abazajian K., et al. (the SDSS Collaboration) 2003, AJ, 126, 2081
- Basser P., 1995, NMR in Biomedical Imaging, 8, 333
- Bertschinger E., 1985, ApJS, 58, 1
- Beucher S., Lantuejoul C., 1979, in Proceedings International Workshop on Image Processing, CCETT/IRISA, Rennes, France
- Beucher S., Meyer F., 1993, Mathematical Morphology in Image Processing. Marcel Dekker, New York
- Blumenthal G. R., da Costa L. N., Goldwirth D. S., Lecar M., Piran T., 1992, ApJ, 388, 234
- Bond J. R., Kofman L., Pogossyan D., 1996, Nature, 380, 603
- Brunino R., Trujillo I., Pearce F. R., Thomas P. A., 2007, MNRAS, 375, 184
- Ceccarelli L., Padilla N. D., Valotto C., Lambas D. G., 2006, MNRAS, 373, 1440
- Ceccarelli L., Paz D., Lares M., Padilla N., Lambas D. G., 2013, MNRAS, 434, 1435
- Chincarini G., Rood H. J., 1975, Nature, 257, 294
- Colberg J. M., Pearce F., et al. 2008, MNRAS, 387, 933

- Colberg J. M., Sheth R. K., Diaferio A., Gao L., Yoshida N., 2005, MNRAS, 360, 216
- Colless M., et al. (the 2dFGRS Team), 2001, MNRAS, 328, 1039
- Colless M., et al. (the 2dFGRS Team), 2003, VizieR Online Data Catalog, 7226
- Croton D. J., et al. 2004, MNRAS, 352, 828
- Dubinski J., da Costa L. N., Goldwirth D. S., Lecar M., Piran T., 1993, ApJ, 410, 458
- Einasto J., Joeveer M., Saar E., 1980a, MNRAS, 193, 353
- Einasto J., Joeveer M., Saar E., 1980b, Nature, 283, 47
- Forero-Romero J. E., Hoffman Y., Gottlöber S., Klypin A., Yepes G., 2009, MNRAS, 396, 1815
- Foster C., Nelson L. A., 2009, ApJ, 699, 1252
- Gottlöber S., Lokas E. L., Klypin A., Hoffman Y., 2003, MNRAS, 344, 715
- Gregory S. A., Thompson L. A., 1978, ApJ, 222, 784
- Hahn O., Porciani C., Carollo C. M., Dekel A., 2007, MNRAS, 375, 489
- Hoffman Y., Metuki O., Yepes G., Gottlöber S., Forero-Romero J. E., Libeskind N. I., Knebe A., 2012, MNRAS, 425, 2049
- Hoffman Y., Shaham J., 1982, ApJL, 262, L23
- Hoyle F., Vogeley M. S., 2004, ApJ, 607, 751
- Icke V., 1984, MNRAS, 206, 1P
- Jarosik N., Bennett C. L., et al. 2011, ApJS, 192, 14
- Kauffmann G., Fairall A. P., 1991, MNRAS, 248, 313
- Kirshner R. P., Oemler Jr. A., Schechter P. L., Shectman S. A., 1981, ApJL, 248, L57
- Kirshner R. P., Oemler Jr. A., Schechter P. L., Shectman S. A., 1987, ApJ, 314, 493
- Klypin A., Gottlöber S., Kravtsov A. V., Khokhlov A. M., 1999, ApJ, 516, 530
- Klypin A. A., Trujillo-Gomez S., Primack J., 2011, ApJ, 740, 102
- Libeskind N. I., Hoffman Y., Forero-Romero J., Gottlöber S., Knebe A., Steinmetz M., Klypin A., 2013, MNRAS, 428, 2489
- Martel H., Wasserman I., 1990, ApJ, 348, 1
- Micheletti D., et al. 2014, ArXiv e-prints
- Müller V., Arbabi-Bidgoli S., Einasto J., Tucker D., 2000, MNRAS, 318, 280
- Nadathur S., Hotchkiss S., 2014, MNRAS, 440, 1248
- Neyrinck M. C., 2008, MNRAS, 386, 2101
- Neyrinck M. C., Falck B. L., Szalay A. S., 2013, ArXiv e-prints
- Pan D. C., Vogeley M. S., Hoyle F., Choi Y.-Y., Park C., 2012, MNRAS, 421, 926
- Patiri S. G., Betancort-Rijo J., Prada F., 2006, MNRAS, 368, 1132
- Patiri S. G., Prada F., Holtzman J., Klypin A., Betancort-Rijo J., 2006, MNRAS, 372, 1710
- Platen E., van de Weygaert R., Jones B. J. T., 2007, MNRAS, 380, 551
- Plionis M., Basilakos S., 2002, MNRAS, 330, 399
- Regos E., Geller M. J., 1991, ApJ, 377, 14
- Ricciardelli E., Quilis V., Planelles S., 2013, MNRAS, 434, 1192
- Riebe K., Partl A. M., Enke H., Forero-Romero J., Gottloeber S., Klypin A., Lemson G., Prada F., Primack J. R., Steinmetz M., Turchaninov V., 2011, ArXiv e-prints
- Rojas R. R., Vogeley M. S., Hoyle F., Brinkmann J., 2005, ApJ, 624, 571
- Schaap W. E., van de Weygaert R., 2000, A&A, 363, L29
- Shandarin S., Feldman H. A., Heitmann K., Habib S., 2006, MNRAS, 367, 1629
- Sutter P. M., Lavaux G., Hamaus N., Pisani A., Wandelt B. D., Warren M. S., Villaescusa-Navarro F., Zivick P., Mao Q., Thompson B. B., 2014, ArXiv e-prints
- Sutter P. M., Lavaux G., Wandelt B. D., Weinberg D. H., 2012, ApJ, 761, 44
- Sutter P. M., Lavaux G., Wandelt B. D., Weinberg D. H., Warren M. S., 2014, MNRAS, 438, 3177
- Tikhonov A. V., 2006, Astronomy Letters, 32, 727
- Tikhonov A. V., 2007, Astronomy Letters, 33, 499
- van de Weygaert R., van Kampen E., 1993, MNRAS, 263, 481
- von Benda-Beckmann A. M., Müller V., 2008, MNRAS, 384, 1189
- York D. G., et al. (the SDSS Collaboration), 2000, AJ, 120, 1579
- Zel'dovich Y. B., 1970, A&A, 5, 84

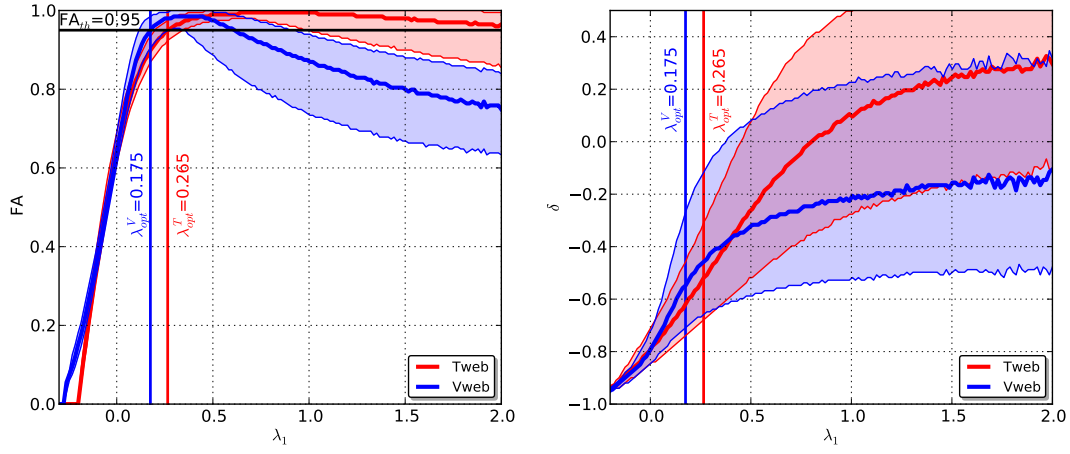


**Figure 1.** Distributions of the fractional anisotropy (left panel) and the density field (right panel) with respect to the eigenvalue  $\lambda_1$  for each web scheme (Tweb, red lines. Vweb, blue lines) as calculated over all cells of the grid. Thick central lines correspond with the median and filled regions with the 50% of the distribution.

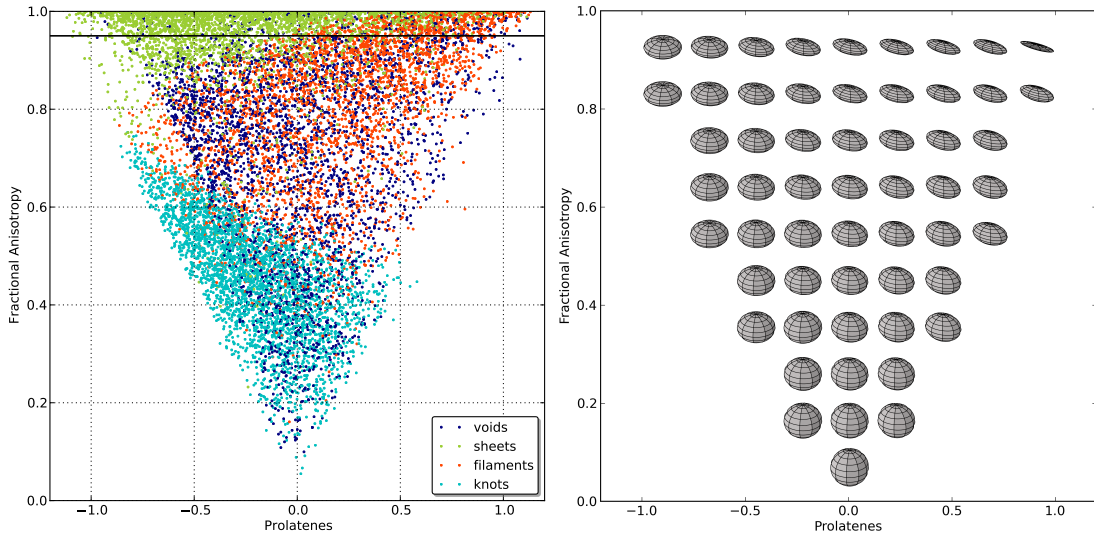


**Figure 2.**



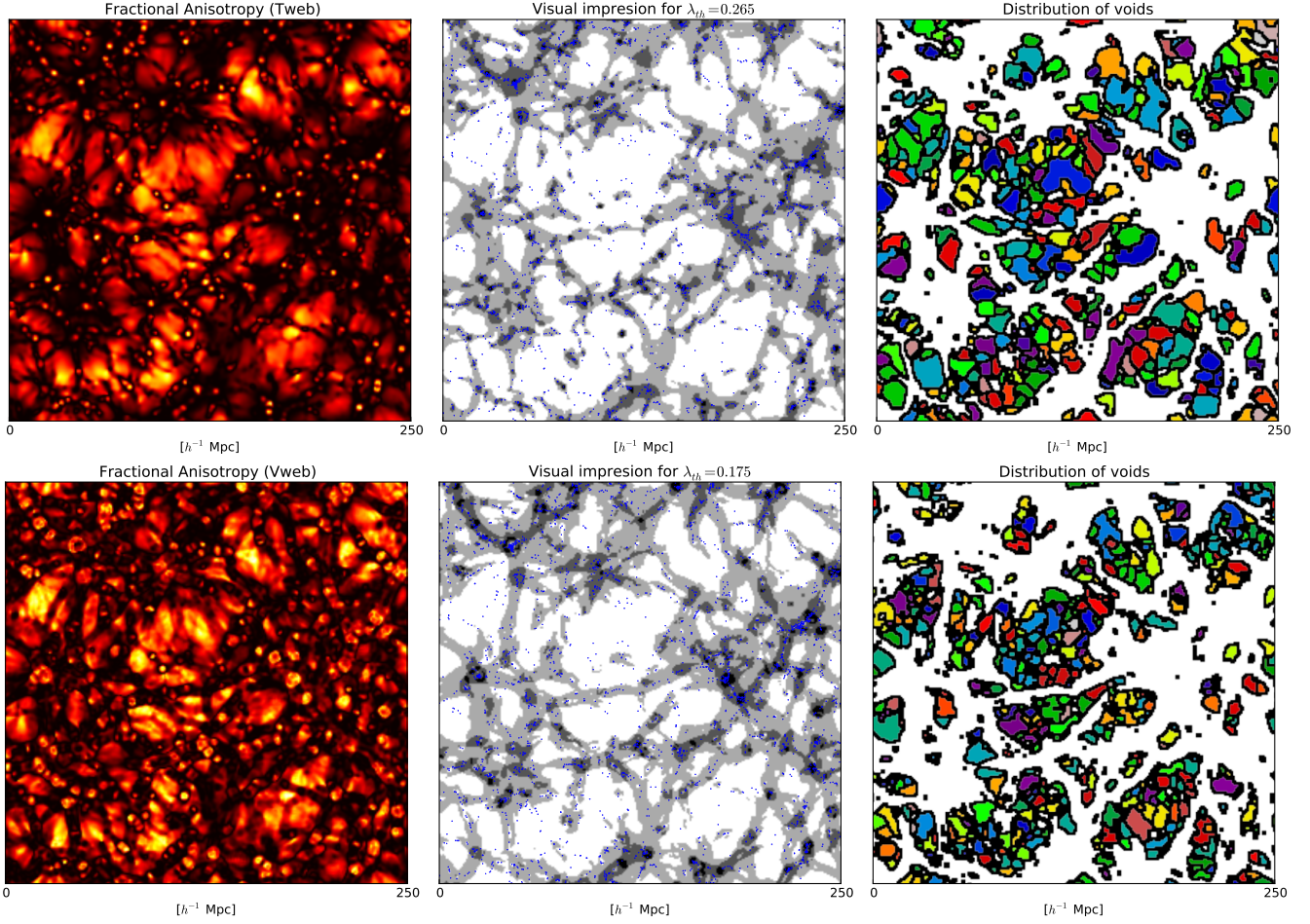


**Figure 3.** Left panels show the visual impression of the Cosmic Web for each web scheme (T-web, upper panels. V-web, middle panels. Density, lower panels). It can be noticed each environment sketched such that voids corresponds to white, sheets to gray, filaments to dark gray and knots to black regions. Right panels show the fractional anisotropy field for the same slide of the simulation and for each web scheme. Black regions correspond to the maxim value, i.e. FA=1, while white and light yellow regions to FA=0. It is worth noting the degeneration of low values of FA for knots and central regions of voids, thus indicating a high isotropy for both processes. In the same way, high values of FA ( $FA \lesssim 1$ ) are consistent the anisotropic geometry exhibited by filaments and very flat sheets.

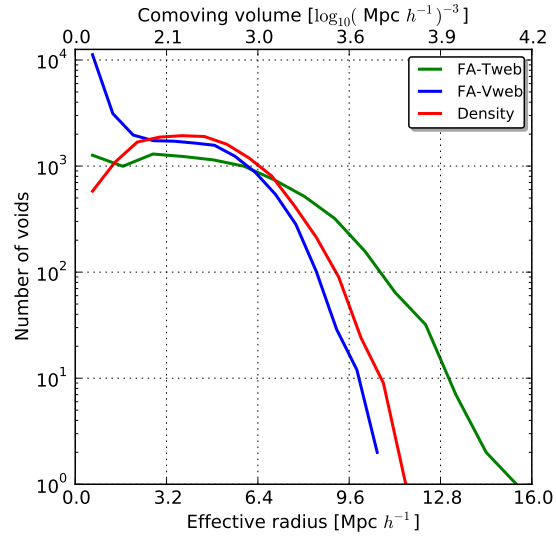


**Figure 4.** Volume functions of voids catalogued by each used scheme. Left panel (watershed transform over the FA field of the T-web scheme). Central panel (over the FA field of the V-web scheme). Right panel (over the density field). Gray curves correspond to voids without boundary removal whereas black curves are associated to voids merged through boundary removal process. Dotted lines correspond to original continuous fields, while segmented lines correspond to fields with a 1st-order median filtering and continuous lines to a 2nd-order median filtering.



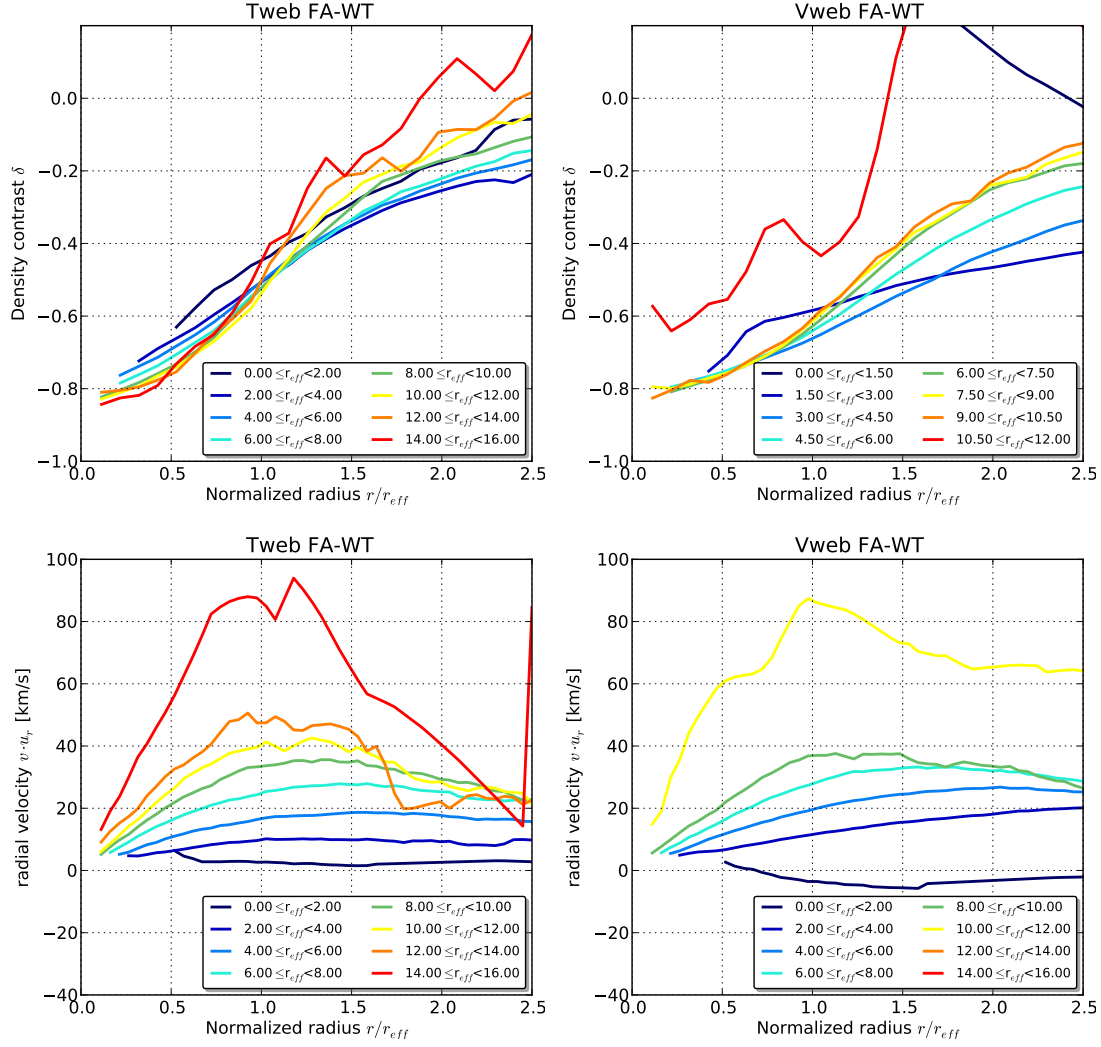


**Figure 5.** Density and velocity profiles of voids for each finding scheme.